The Astrophysical Journal, 691:661–671, 2009 January 20 doi:10.1088/0004-637X/691/1/661

THE EFFECT OF PROGENITOR AGE AND METALLICITY ON LUMINOSITY AND ^{56}Ni YIELD IN TYPE Ia SUPERNOVAE

D. A. Howell[1,2,3], M. Sullivan[1,4], E. F. Brown[5], A. Conley[1], D. Le Borgne[6], E. Y. Hsiao[7], P. Astier[8], D. Balam[7], C. Balland[8,9], S. Basa[10], R. G. Carlberg[1], D. Fouchez[11], J. Guy[8], D. Hardin[8], I. M. Hook[4], R. Pain[8], K. Perrett[1], C. J. Pritchet[7], N. Regnault[8], S. Baumont[8], J. Le Du[11], C. Lidman[12], S. Perlmutter[13,14], N. Suzuki[13], E. S. Walker[4], and J. C. Wheeler[15]

[1] Department of Astronomy and Astrophysics, University of Toronto, 50 St. George Street, Toronto, ON M5S 3H8, Canada
[2] Las Cumbres Observatory Global Telescope Network, 6740 Cortona Dr., Suite 102, Goleta, CA 93117, USA
[3] Department of Physics, University of California, Santa Barbara, Broida Hall, Mail Code 9530, Santa Barbara, CA 93106-9530, USA
[4] University of Oxford Astrophysics, Denys Wilkinson Building, Keble Road, Oxford OX1 3RH, UK
[5] Department of Physics & Astronomy, National Superconducting Cyclotron Laboratory, and the Joint Institute for Nuclear Astrophysics, Michigan State University, East Lansing, MI 48824, USA
[6] Institut d'Astrophysique de Paris, UMR7095 CNRS, UPMC, 98 bis Boulevard Arago, 75014 Paris, France
[7] Department of Physics and Astronomy, University of Victoria, P.O. Box 3055, Victoria, BC V8W 3P6, Canada
[8] LPNHE, CNRS-IN2P3 and University of Paris VI & VII, 75005 Paris, France
[9] Univ. Paris-Sud, Orsay, F-91405, France
[10] Laboratoire d'Astrophysique de Marseille, Pôle de l'Etoile Site de Château-Gombert, 38, rue Frédéric Joliot-Curie, 13388 Marseille cedex 13, France
[11] CPPM, CNRS-Luminy, Case 907, 13288 Marseille Cedex 9, France
[12] ESO, Alonso de Cordova, 3107, Vitacura Casilla 19001, Santiago 19, Chile
[13] Lawrence Berkeley National Laboratory, Mail Stop 50-232, Lawrence Berkeley National Laboratory, 1 Cyclotron Road, Berkeley, CA 94720, USA
[14] Department of Physics, University of California, 366 LeConte Hall MC 7300, Berkeley, CA 94720-7300, USA
[15] Department of Astronomy, University of Texas, RLM 5.208, Austin, TX 78712-1081, USA
Received 2008 April 25; accepted 2008 September 27; published 2009 January 16

ABSTRACT

Timmes et al. found that metallicity variations could theoretically account for a 25% variation in the mass of ^{56}Ni synthesized in Type Ia supernovae (SNe Ia), and thus account for a large fraction of the scatter in observed SN Ia luminosities. Higher-metallicity progenitors are more neutron rich, producing more stable burning products relative to radioactive ^{56}Ni. We develop a new method for estimating bolometric luminosity and ^{56}Ni yield in SNe Ia and use it to test the theory with data from the Supernova Legacy Survey. We find that the average ^{56}Ni yield does drop in SNe Ia from high-metallicity environments, but the theory can only account for 7%–10% of the dispersion in SN Ia ^{56}Ni mass, and thus luminosity. This is because the effect is dominant at metallicities significantly above solar, whereas we find that SN hosts have predominantly subsolar or only moderately above-solar metallicities. We also show that allowing for changes in O/Fe with the metallicity [Fe/H] does not have a major effect on the theoretical prediction of Timmes et al., so long as one is using the O/H as the independent variable. Age may have a greater effect than metallicity—we find that the luminosity-weighted age of the host galaxy is correlated with ^{56}Ni yield, and thus more massive progenitors give rise to more luminous explosions. This is hard to understand if most SNe Ia explode when the primaries reach the Chandrasekhar mass. Finally, we test the findings of Gallagher et al. that the residuals of SNe Ia from the Hubble diagram are correlated with host galaxy metallicity, and we find no such correlation.

Key words: galaxies: abundances – galaxies: fundamental parameters – galaxies: high-redshift – supernovae: general – surveys

Online-only material: color figures

1. INTRODUCTION

Type Ia supernovae (SNe Ia) make excellent cosmological standard candles (Riess et al. 1998; Perlmutter et al. 1999), though only after they are empirically calibrated based on their lightcurve shape (Phillips 1993) and color (Riess et al. 1996). There is consensus that the luminosity of SNe Ia arises from the radioactive decay of ^{56}Ni to ^{56}Co, and finally to ^{56}Fe (Truran et al. 1967; Colgate & McKee 1969). Therefore, the primary variable controlling supernovae (SNe) luminosity is the amount of ^{56}Ni synthesized during the explosion, though as second-order effects the location of the ^{56}Ni (e.g., Branch & Khokhlov 1995; Nugent et al. 1997; Pinto & Eastman 2000a), the opacity of the overlying material (e.g., Khokhlov et al. 1993; Pinto & Eastman 2000b; Mazzali et al. 2001; Kasen & Woosley 2007), and asymmetries in the ejecta (Howell et al. 2001; Kasen et al. 2004) can redistribute the energy in wavelength, time, or space. However, because SNe Ia are largely spherical (Wang et al. 1996; Leonard et al. 2005), the bulk of ^{56}Ni is located near the center, and simple assumptions about the opacity are a reasonable approximation, Arnett's Rule (Arnett 1979, 1982) can be used to empirically estimate the ^{56}Ni mass from the optical-infrared lightcurve to an accuracy of 5%–15% (Stritzinger et al. 2006; Blinnikov et al. 2006).

The variables that control the yield of ^{56}Ni in a SN Ia are not well understood, although several factors are known to be important. Iron-peak elements are produced when burning occurs in a state of nuclear statistical equilibrium, which happens at the highest densities near the center of the white dwarf. If this burning occurs in a neutron-rich region, more neutron-rich, stable, iron-peak elements like ^{58}Ni and ^{54}Fe will be produced relative to ^{56}Ni. Since main-sequence stars with higher metallicity

abundances produce white dwarfs with more of the neutron-rich nuclides ^{22}Ne and ^{56}Fe, Timmes et al. (2003, hereafter TBT03) hypothesized that high-metallicity progenitors will produce less ^{56}Ni and therefore less luminous SNe Ia.

In the absence of any identified SN Ia progenitor, the best one could hope for is to see traces of the progenitor's metallicity in the unburned outer layers of the SN by looking at Type Ia spectra from only a few days after the explosion in the UV (Höflich et al. 1998; Lentz et al. 2001). Unfortunately, the difficulty of obtaining UV spectra has prevented the gathering of a statistically significant sample of spectra from the earliest phases. In the case of local SNe Ia it has not been possible to schedule HST quickly enough (Foley et al. 2008; Sauer et al. 2008). Another option is to observe higher redshift SNe Ia in the restframe UV, though their faintness at such early epochs relative to their host galaxy makes observations earlier than one week before maximum light difficult (Ellis et al. 2008). More importantly, even when UV spectra have been obtained their theoretical interpretation is not straightforward (Ellis et al. 2008).

Since a true progenitor metallicity has so far been unobtainable,[16] the next best thing is to determine the average metallicity in the environment of the SN. The two most commonly used approaches have been to measure spectroscopic line indices (Hamuy et al. 2000; Gallagher et al. 2008) or ratios (Gallagher et al. 2005) to determine a global average host galaxy metallicity, or to take advantage of the fact that galaxies often have metallicity gradients, and study projected galactocentric offset as a proxy for metallicity (Wang et al. 1997; Ivanov et al. 2000; Gallagher et al. 2005). The drawbacks of the spectroscopic line techniques are that they require complicated corrections for contamination by emission, and that the interpretation of the line ratios as metallicity requires mapping observations to a sometimes-incongruous grid of theoretical models (e.g., Trager et al. 2000; Kewley & Dopita 2002; Gallagher et al. 2008). Furthermore, the line ratios only represent the current average metallicity—the metallicity when the SN Ia progenitor formed may have been different. In addition, high signal-to-noise ratio (S/N) spectra are required, and important lines like Hα are redshifted into the IR at $z > 0.5$. These factors limit the possible sample size of such a data set. The drawbacks of the offset technique are that projection effects can be confusing (Wang et al. 1997; van den Bergh 1997), as is differential reddening between SNe near and far from galaxy centers (Hatano et al. 1998), and Malmquist-like effects (Howell et al. 2000). Further complications include that different galaxy types have different metallicity gradients, and the current location of the SN may not be representative of where the progenitor formed.

With the exception of Gallagher et al. (2008), hereafter G08, none of the above studies found a significant correlation between metallicity and SN Ia properties, although it is not clear whether this is caused by the lack of an effect or whether the techniques used so far do not have the required level of precision. G08 compared absorption-line strengths of 29 E/S0 galaxies which hosted SNe Ia to a grid of models and found that galaxies with high iron abundances host less luminous supernovae. They went on to conclude that age played a greater role, since galaxies with characteristic ages greater than 5 Gyr produce $\sim$ 1 mag fainter SNe Ia in V. Their most controversial finding is that the MLCS lightcurve fitter could not fully correct for SN luminosities in different metallicity environments; when Hubble residuals were correlated with metallicity, they found a significant trend. But since these findings are based on a small sample size, rely on an uncertain metallicity determination techniques, and rely entirely on a lightcurve fitter (MLCS2k2; Jha et al. 2007) that has recently shown spurious systematic trends with Hubble residuals (Conley et al. 2007), they are worth scrutinizing with independent techniques and a much larger sample size.

Here, we use an independent approach not previously applied to testing SN luminosity–metallicity relations—we estimate the host galaxy metallicity from its mass using spectral energy distribution (SED) fits to the host galaxy photometry and the Tremonti et al. (2004) mass–metallicity relation.[17]

Another discriminator of the metallicity effect is that it may cause luminosity differences as a function of redshift, since cosmic metallicity is increasing with time (e.g., Savaglio et al. 2005). This is in contrast to many other possible contributors to SN Ia luminosity (for example, white dwarf core density) which would not be expected to change with redshift. We perform the first tests of the effect of inferred metallicity on SN Ia nickel mass with high redshift supernovae, using data from the Supernova Legacy Survey (SNLS).

In this paper, we first update the TBT03 SN Ia metallicity–^{56}Ni mass relation to account for the fact that O/Fe can vary as a function of Fe/H (Section 2). Then we test the theory using data from the SNLS. To do this, in Section 3.1 we estimate host galaxy masses from PEGASE-2 model fits to $u_M g_M r_M i_M z_M$ (subscripts denote Megacam filters) host galaxy photometry. In Section 3.2, we use galaxy mass–metallicity relations to estimate host metallicities. In Section 3.3, we determine SN ^{56}Ni mass from SNLS photometry. Finally, we test the theory with the data in Section 4 and discuss the implications in Section 5.

2. THE VARIATION OF ^{56}Ni MASS WITH PROGENITOR METALLICITY

TBT03 note that a white dwarf's ^{22}Ne abundance should trace its progenitor star's O abundance since C, N, and O are converted to ^{14}N during hydrogen burning (^{14}N(p,γ) is the slowest step in the CNO cycle), and this ^{14}N is converted to ^{22}Ne during core helium burning. Since ^{22}Ne is neutron rich, its presence during the burning in the Type Ia supernova favors the production of stable, neutron-rich nuclides like ^{58}Ni and ^{54}Fe at the expense of radioactive ^{56}Ni, the decay of which powers the supernova. Thus, more metal-rich progenitors are expected to produce dimmer SNe Ia.

The progenitor star's abundance of ^{56}Fe is also important, but one possible limitation of TBT03 is that metallicity was treated as a single variable, i.e., TBT03 make the simplifying assumption that O/Fe is constant relative to Fe/H. In reality, O/Fe varies as a function of Fe/H (with a great deal of scatter), at least in the solar neighborhood (e.g., Wheeler et al. 1989), and the degree of variation is expected to vary with the history of star formation. Here, we refine the estimate of the mass of ^{56}Ni to include changes in the relative abundances of O and Fe.

TBT03 showed that M_{56}, the mass of ^{56}Ni synthesized in the explosion, depended on the electron abundance Y_e,

$$M_{56} = M_{56}^{0}(58Y_e - 28). \quad (1)$$

[16] Though see Badenes et al. (2008) for a technique for determining progenitor metallicity from a SN Ia remnant by estimating the neutron excess from the Mn/Cr ratio.

[17] Note that Prieto et al. (2008) studied the relative rates of all types of SNe in different metallicity hosts by using the Tremonti et al. (2004) data, not the relation—they studied historical SNe that also had host galaxy spectra from the Sloan Digital Sky Survey (SDSS).

Here, M_{56}^0 is the mass of ^{56}Ni synthesized at an electron abundance $Y_e = 1/2$, i.e., for a pure C–O white dwarf. It does not include material that has been neutronized by in situ electron captures at high densities. To a good approximation, we can consider the white dwarf to consist of ^{12}C, ^{16}O, ^{22}Ne, and ^{56}Fe. The electron abundance is then

$$Y_e = \tfrac{1}{2}(1 - 22Y_{\rm Ne} - 56Y_{\rm Fe}) + 10Y_{\rm Ne} + 26Y_{\rm Fe}, \quad (2)$$

where $Y_i = X_i/A_i$ is the abundance of nuclide i, X_i and A_i being the mass fraction and atomic mass number, respectively. Since ^{22}Ne is derived from the aboriginal CNO abundances of the progenitor main-sequence star, $Y_{\rm Ne} = Y_{\rm O} + Y_{\rm N} + Y_{\rm C}$. Nitrogen is a secondary element, and we therefore write $Y_{\rm N} = Y_{\rm O}\,[1 + ({\rm N/O})]$, with $({\rm N/O}) = 0.0316 + 126({\rm O/H})$ (Vila Costas & Edmunds 1993). This formula includes the secondary production of nitrogen at high metallicity and agrees with derived abundance ratios from the Sloan Digital Sky Survey (SDSS) (Liang et al. 2006). Carbon is a primary element, but is mostly produced in lower-mass stars, which tends to make the ratio (C/Fe) nearly constant at subsolar metallicities, at least down to [Fe/H] $\gtrsim -2$ (Chiappini et al. 2003; Bensby & Feltzing 2006), and there is evidence that [C/Fe] decreases slightly at super-solar metallicity in the thin disk (Bensby & Feltzing 2006). We take (C/Fe) = 8.7, its solar value (Asplund et al. 2005).

Writing $Y_{\rm O} = X_{\rm H}({\rm O/H})$ and $Y_{\rm Fe} = X_{\rm H}({\rm Fe/H})$, setting $X_{\rm H} = 0.7392$ (Asplund et al. 2005), and inserting Equation (2) into Equation (1) gives

$$\frac{M_{56}}{M_{56}^0} = 1 - 58\left\{0.763\left(\frac{\rm O}{\rm H}\right) + 93.1\left(\frac{\rm O}{\rm H}\right)^2 + 7.92\left(\frac{\rm Fe}{\rm H}\right)\right\}. \quad (3)$$

The factor of 58 comes from the assumption that the two dominant nuclides in the burn to nuclear statistical equilibrium are ^{56}Ni and ^{58}Ni. In actuality ^{54}Fe is also present, and the ratio of ^{54}Fe to ^{58}Ni depends on the thermal conditions of the explosion (TBT03), so that the coefficient varies between 58 and 54. As shown by TBT03, this results in a small scatter ($< 1\%$ at $Z = 3Z_\odot$) about the relation in Equation (3).

The two abundance ratios in Equation (3) are correlated, albeit with a great deal of scatter. We can therefore eliminate Fe/H in favor of O/H and the coefficients from the relation between [Fe/H] (the "metallicity") and [O/Fe]. Here, we are using the standard notation [A/B] $\equiv \log({\rm A/B}) - \log({\rm A/B})_\odot$. Ramírez et al. (2007) fit a set of linear relations, [O/Fe] $= a + b$ [Fe/H], for the thin disk, the thick disk, and the halo (see Table 1). We therefore write $({\rm Fe/H}) = ({\rm Fe/H})_\odot\, 10^{[{\rm Fe/H}]}$, use the linear relation between [O/Fe] and [Fe/H] and the identity [O/Fe] = [O/H] − [Fe/H] to obtain [Fe/H] $= ([{\rm O/H}] - a)/(1 + b)$, and insert the solar photospheric abundances (Asplund et al. 2005), $\log({\rm O/H})_\odot = -3.34$ and $\log({\rm Fe/H})_\odot = -4.55$, into Equation (3) to obtain

$$\frac{M_{56}}{M_{56}^0} = 1 - 0.044\left[\frac{({\rm O/H})}{10^{-3}}\right]\left\{1 + 0.122\left[\frac{({\rm O/H})}{10^{-3}}\right] + 10^{-(0.19+0.53b+a)/(1+b)}\left[\frac{({\rm O/H})}{10^{-3}}\right]^{-b/(1+b)}\right\}. \quad (4)$$

For many purposes, it is more convenient to work directly with [Fe/H] as the primary variable. We therefore write

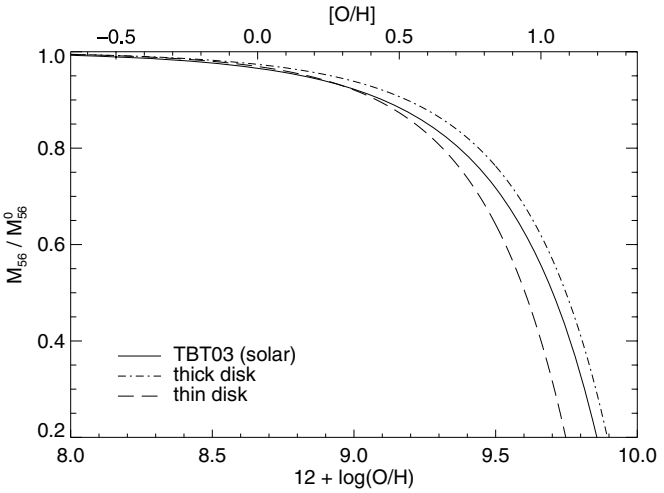

Figure 1. Theoretically expected variation in M_{56}, the mass of ^{56}Ni synthesized, as a function of O/H. The solid line shows the prediction of TBT03, which fixed [O/Fe] = 0. The other lines show the prediction when O/Fe varies according to linear relations Ramírez et al. (2007) fitted to the thin (*dashed lines*) and thick (*dot-dashed lines*) disk. For illustrative purposes, we show each over a two decade span in metallicity as plotted in TBT03, though the thick and thin disk relations were derived over narrower metallicity ranges (see Table 1), and SN hosts do not have average metallicities spanning this full range (Section 4).

Table 1
[O/Fe] for Different Populations

	a	b	Range
Thin disk	0.096 ± 0.004	-0.327 ± 0.016	$-1.0 <$ [Fe/H] < -0.3
Thick disk	0.370 ± 0.027	-0.121 ± 0.043	$-0.8 <$ [Fe/H] < 0.3
Halo	0.388 ± 0.049	-0.048 ± 0.071	$-1.4 <$ [Fe/H] < -0.4

Notes. Coefficients of the fit [O/Fe] $= a + b$ [Fe/H] from Ramírez et al. (2007).

$({\rm O/H}) = ({\rm O/H})_\odot 10^{[{\rm O/Fe}]+[{\rm Fe/H}]}$ and use the linear relation between [O/Fe] and [Fe/H] to obtain

$$\frac{M_{56}}{M_{56}^0} = 1 - 0.020 \times 10^{a+(1+b)[{\rm Fe/H}]}\{1 + 0.056 \times 10^{a+(1+b)[{\rm Fe/H}]} + 0.64 \times 10^{-a-b[{\rm Fe/H}]}\}. \quad (5)$$

In both Equations, (4) and (5), setting $a = b = 0$ will give the case of a system where O/Fe is held at its solar value. Figure 1 shows Equation (4) with coefficients taken from Ramírez et al. (2007) for the thin disk (*dashed line*) and thick disk (*dash-dotted line*). We also show, for comparison, the relation when O/Fe is fixed at its solar value (*solid line*). This last curve differs slightly from that in TBT03 because we are using the Asplund et al. (2005) abundances for the solar composition, and we include the secondary production of ^{14}N. This scaling is appropriate for the Milky Way, but supernova hosts may have a different metallicity history. This does not appear to be much of a concern, however, since the differences between the predictions using the thick and thin disk parameters are small for [O/H] < 0.5. We conclude from this section that O/Fe variations can safely be neglected at the level of precision of the TBT03 theory, for the relevant range, [O/H] < 0.5. We note from Figure 1 that TBT03 would have predicted a variation of nickel mass with metallicity of less than 10% had they restricted their considerations to the observationally relevant range of [O/H] < 0.5 that corresponds to [Fe/H] < 0.6 in the thin disk model.

3. METHOD

3.1. Estimating Host Galaxy Masses

To test the TBT03 theory, we must determine host galaxy metallicities, and to do that we first determine galaxy masses from model SED fits to SNLS photometry. Following the procedure outlined in Sullivan et al. (2006), we used the code Z-PEG (Le Borgne & Rocca-Volmerange 2002) to fit PEGASE.2 (Fioc & Rocca-Volmerange 1997, 1999) models to host galaxy $u_M g_M r_M i_M z_M$ photometry from the SNLS to determine their masses and star-formation rates (SFRs). We extend the analysis of Sullivan et al. (2006) to include data from the SNLS third-year cosomology sample (M. Sullivan 2009, in preparation, A. Conley 2009, in preparation, J. Guy 2009, in preparation).

The SNLS revisits four one-degree fields five times per lunation for the 5–6 lunations per year that each field is visible. Images with seeing $< 0.8''$ and no SN light are combined to provide a deep, multi-year reference image from which the host galaxy properties are measured SN types and host galaxy redshifts were determined from Gemini, VLT, and Keck spectroscopy (Howell et al. 2005; Bronder et al. 2008; Baumont et al. 2008; Ellis et al. 2008). We categorize each galaxy by its SFR per unit mass (specific SFR; sSFR) into strong star formers ($\log(\mathrm{sSFR}) > -9.5$), weak star formers ($-12 > \log(\mathrm{sSFR}) > -9.5$), and passive galaxies with no measurable SFR ($\log(\mathrm{sSFR}) < -12$). Here, SFR is the average SFR over the last 0.5 Gyr, which is estimated from the optical SED fitting. We assign errors corresponding to the range of masses that can be fit within a model given the photometric errors, or the scatter between acceptable model fits in terms of χ^2, whichever is larger. As in Sullivan et al. (2006), we only use SNe at $z \leqslant 0.75$ where the SNLS sample is relatively complete. For more information on the SNLS, including discoveries, the photometric system, and SN typing, see Astier et al. (2006).

3.2. Estimating Metallicity

To determine average host galaxy metallicities we use the Tremonti et al. (2004) correlation between host galaxy stellar mass and gas phase O/H as determined from 53,000 galaxies in the SDSS. There is a 0.1 dex scatter in this relationship. For galaxies with $\log M_* < 8.4$ we use the low-mass extension of Lee et al. (2006). Both of these relationships were derived for zero redshift—Savaglio et al. (2005) find that higher-redshift galaxies have lower average gas-phase metallicities. They give an "effective Mass" versus redshift relation (Savaglio et al. (2005), Equation 9), which we use here to adapt the Tremonti et al. (2004) and Lee et al. (2006) relations to the redshifts of our galaxies.

Technically the Tremonti et al. (2004) relationship only covers gas-phase metallicity, and is not guaranteed to be applicable in elliptical galaxies, where there is generally little cold gas. Still, there are several reasons not to dismiss the sample of passive galaxies from this analysis. First, the amount of star formation in these galaxies is inferred from their broadband colors, not from spectroscopy or morphology, so the presence of gas is not ruled out. Second, because the mechanism for retaining metals is the depth of the galaxy gravitational potential well, one might still expect ellipticals to follow this trend, independent of the presence of gas. The SN progenitor was born when there was star formation, and thus much more gas in the galaxy. Finally, we caution that stellar metallicity and gas-phase metallicity are not identical, though they are correlated (e.g., Cid Fernandes et al. 2005).

3.3. Estimating ^{56}Ni Mass

The mass of ^{56}Ni can be estimated from the peak bolometric luminosity and the rise time of a SN Ia using Arnett's Rule (Arnett 1979, 1982) that the luminosity radiated at maximum light is approximately equal to the energy deposited by radioactive decay,

$$M_{\mathrm{Ni}} = \frac{L_{\mathrm{bol}}}{\gamma \dot{S}(t_R)},$$

where γ is the ratio of bolometric to radioactivity luminosities, near unity (e.g., Branch 1992; Höflich & Khokhlov 1996; Blinnikov et al. 2006). Here, we adopt a value of 1.2 ± 0.1 (Nugent et al. 1995; Branch & Khokhlov 1995) to be consistent with previous SNLS work (Howell et al. 2006), though a global change to this number does not affect our conclusions. $\dot{S}$ is the radioactivity luminosity per solar mass of ^{56}Ni from its decay to ^{56}Co and subsequent decay to ^{56}Fe,

$$\dot{S} = 7.74 \times 10^{43} e^{-t_R/8.8} + 1.43 \times 10^{43} \times [e^{-t_R/111} - e^{-t_R/8.8}] \ \mathrm{erg\ s^{-1}}\ M_\odot^{-1}.$$

Here t_R is the time in days for the supernova to rise from explosion to maximum light: $t_R = s \times 19.5$ days (Riess et al. 1999; Conley et al. 2006), where s is the "stretch," a scaling factor for the time axis of the SN lightcurve that correlates with luminosity (Perlmutter et al. 1997; Conley et al. 2008). Note that simply taking the mass difference between ^{56}Ni and ^{56}Co, as some authors have done, will overestimate the energy production. The heating from the decay of ^{56}Ni is primarily from the radiative decay of the 1.7 MeV nuclear level in ^{56}Co (Junde 1999). We include contributions from the positron decay branching in the heating from the decay of ^{56}Co (Colgate et al. 1980).

The least straightforward part of determining ^{56}Ni mass from SN Ia lightcurves is estimating the bolometric luminosity from incomplete data. For rare, very well-observed supernovae with data spanning much of the UVOIR (ultraviolet, optical, infrared) region, all of the flux can be added, and only a small correction is necessary for missing data (e.g., Contardo et al. 2000; Stritzinger et al. 2006). However, this has to date only been possible for small numbers (~ 15) of low-redshift supernovae. Because the best-observed supernovae tend to be the closest and brightest, and thus not in the Hubble flow, these SNe often have uncertain distances and luminosities.

Other authors have used the luminosity in a single band, combined with a bolometric correction, to estimate the bolometric flux (e.g., Branch 1992; Howell et al. 2006). This allows the study of greater numbers of supernovae, achieving enhanced global accuracy, at the expense of individual accuracy. It also makes possible the study of high redshift supernovae where the restframe NIR is inaccessible.

Bolometric corrections work well at maximum light for SNe Ia because the peak of emission is always in the restframe B band, near 4000 Å (in the absence of strong reddening). Figure 2 (bottom panel) shows a typical SN Ia SED at maximum light (from Hsiao et al. (2007), updated with NIR data). The upper panel shows the cumulative flux as a function of wavelength. Only $\sim 5\%$ of the SN Ia flux is emitted in the UV shortward of the U filter, and less than 10% is emitted in the IR.[18] Since roughly one-quarter of the SN Ia flux is emitted in the B band, and this fraction is relatively constant from SN to SN, it is easy

[18] Our template spans 1000 Å—2.4 μm—since there is no evidence for significant SN Ia flux outside of this range, we assume it to be negligible.

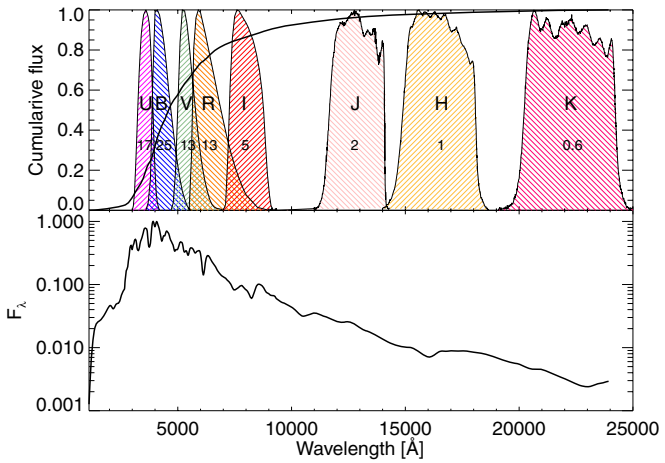

Figure 2. Bottom: the Hsiao et al. (2007) SN Ia maximum-light SED template (plotted on a log-axis), updated to include NIR data. Top: cumulative flux as a function of wavelength. Johnson–Cousins filters are shown with labels corresponding to the percentage of total flux through each. Approximately 3/4 of the flux for a typical SN Ia is radiated in the optical.

(A color version of this figure is available in the online journal.)

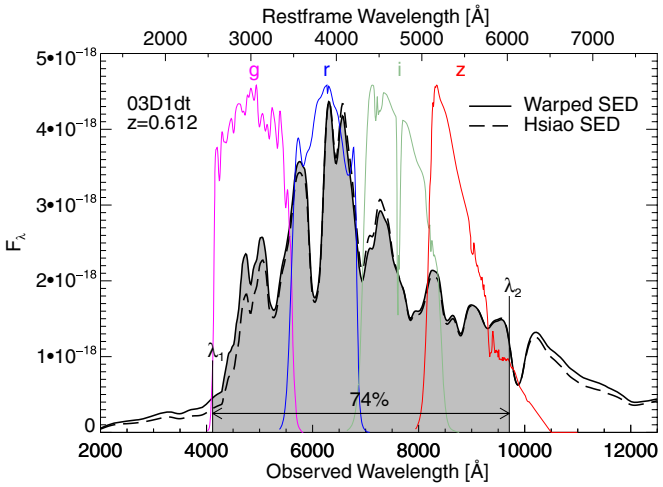

Figure 3. Determination of the bolometric flux for an example SN Ia, SNLS-03D1dt at $z = 0.612$. The dashed line shows the (Hsiao et al. 2007) SED, and the solid line shows it warped to match the observed $g_M r_M i_M z_M$ fluxes. This warped SED is then integrated over the observed region (shaded), from λ_1 to λ_2, arbitrarily defined to start and stop where the bluest and reddest filters are 1/5 of their maximum height. Since this region contains only 74% of the total Hsiao SED bolometric flux (see Figure 2), the integrated flux is divided by 0.74 to obtain the bolometric flux.

(A color version of this figure is available in the online journal.)

to see why the B band is the most commonly used indicator of SN Ia luminosity.

Here, we adopt a new approach to bolometric flux estimation that exploits the excellent multiwavelength coverage of SNLS supernovae. For each SNLS SN Ia, we smoothly adjust (i.e., "warp") the Hsiao SED template so that it has the observed fluxes in $g_M r_M i_M z_M$. We then integrate the template SED over the wavelength interval where we have observations, and correct for the unobserved fraction. We turn this bolometric observed flux into a luminosity using the redshift and a flat cosmology with $H_0 = 70$ km s^{-1} Mpc^{-1} and $\Omega_M = 0.3$. An example is shown in Figure 3.

Note that this process uses much of the same machinery as the SiFTO lightcurve fitter (Conley et al. 2008). The first step, warping the SED to match the observed colors, is identical. But in the next step the methods diverge—SiFTO calculates the restframe flux of SN through another filter, whereas here we calculate the integrated flux over the region spanning all observed filters.

Mathematically, we define f as the fraction of the bolometric flux covered by our observations, such that

$$f = \frac{\int_{\lambda_1}^{\lambda_2} H(\lambda) d\lambda}{\int H(\lambda) d\lambda}, \quad (6)$$

where $H(\lambda)$ is the Hsiao SN Ia SED template, λ_1 is the wavelength at 1/5 the filter height of the bluest filter for which there is data, and λ_2 is the wavelength at 1/5 the filter height of the reddest filter for which there is data. The choice of 1/5 of the filter height as the cutoff is arbitrary—changing it does not affect our results.

We define $S(\lambda)$ as the SED after it is warped to match the observed colors, so that the bolometric flux is

$$F_{\rm bol} = \frac{\int_{\lambda_1}^{\lambda_2} S(\lambda) d\lambda}{f}. \quad (7)$$

Flux errors are given by the SiFTO covariance matrix (see Conley et al. 2008). Errors on the other quantities are

$$\sigma_{\dot{S}} = |-1.4 \times 10^{44} e^{-2.2s} - 2.5 \times 10^{42} e^{-0.18s}| \times \sigma_s \quad (8)$$

Table 2
Parameters of Color Cut

	Color	a	b	c
$U02 - B$	0.1856	−0.0003	−0.1681	0.0790
$U-B$	0.4031	0.1816	−0.0567	0.0477
$V-R$	1.0129	0.1957	−0.5634	0.0646

Notes. SNe Ia rejected if the $B-V$ color is redder than a(color+0.5)+b($s-1$)+c, where s is the stretch (lightcurve width). "$U02$" is a virtual filter useful in k-correcting (Hsiao et al. 2007) high redshift data, defined to be bluer than the U filter (M. Sullivan 2009, in preparation). A $B-V$ and at least one other color was required for all SNe Ia. Cuts were made in as many filters as data were available. The cuts mimic those used in M. Sullivan 2009, in preparation.

$$\sigma_{^{56}\rm Ni} = \sqrt{\left(\frac{1}{\gamma \dot{S}}\right)^2 \sigma_{L_{\rm bol}}^2 + \left(\frac{L_{\rm bol}}{\gamma \dot{S}^2}\right)^2 \sigma_{\dot{S}}^2 + \left(\frac{L_{\rm bol}}{\gamma^2 \dot{S}}\right)^2 \sigma_\gamma^2}. \quad (9)$$

Based on constraints from theory (e.g., Branch 1992; Höflich & Khokhlov 1996), and from estimating ^{56}Ni using different empirical methods (Stritzinger et al. 2006), we adopt $\sigma_\gamma = 0.1$ and generally this term dominates the error budget.

In the absence of dust extinction, one should use the raw absolute magnitude (i.e., not corrected for stretch or color), because this reflects the true luminosity of the SN. The complication is that the observed color is a mixture of reddening due to dust (which should be corrected for), and intrinsic SN color (which should not be corrected). If the color correction were primarily due to normal dust, it would be expected to follow the Milky Way extinction law (Cardelli et al. 1989), but it does not (e.g., Wang et al. 2008; Elias-Rosa et al. 2008; Krisciunas et al. 2007; Conley et al. 2007). There are theoretical reasons to expect, and some evidence, that the majority of SNe Ia suffer little extinction (Hatano et al. 1998; Perlmutter et al. 1999; Phillips et al. 1999; Commins 2004), though some of the reddest outliers surely have significant dust extinction. As our primary result, we chose to make a color cut (M. Sullivan 2009, in preparation) to eliminate the most extincted SNe rather than making an uncertain extinction correction (Conley et al. 2007). The parameters of the color

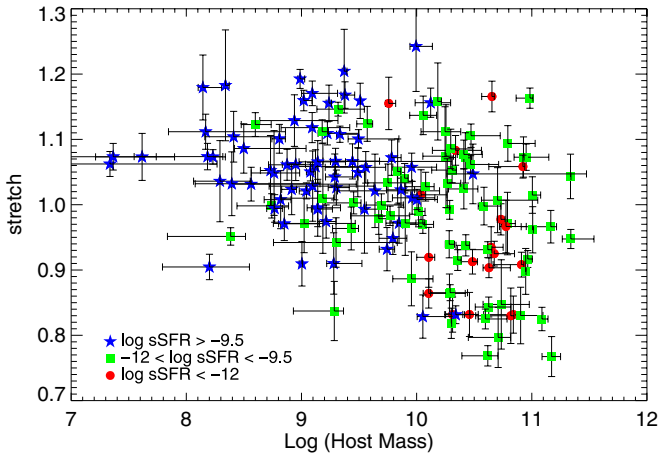

Figure 4. SN relative lightcurve width (stretch) as a function of host galaxy mass determined from fitting PEGASE.2 galaxy models to host galaxy $u_M g_M r_M i_M z_M$ photometry. Circles (red online) have hosts with no detectable star formation (log sSFR < -12), where sSFR is specific star-formation rate. Star symbols (blue) denote strong star formation (log sSFR > -9.5), and squares (green) are in between.

(A color version of this figure is available in the online journal.)

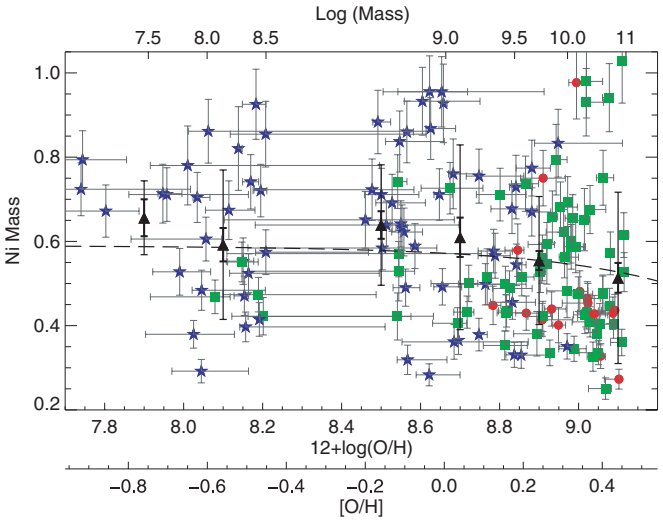

Figure 5. ^{56}Ni mass as a function of inferred average host gas-phase metallicity. The dashed line is the prediction of TBT03 modified to use the thin disk variation in O/Fe as described in Section 2. Points are SNLS SNe Ia with ^{56}Ni mass and inferred average host metallicity determined as described in the text and colored as in Figure 4. Vertical error bars include flux errors, stretch errors, and errors associated with Arnett's Rule. Horizontal error bars include errors from the model fits, but for clarity do not include the 0.1 dex scatter from the Tremonti et al. (2004) relationship. The gap at 12+log(O/H) = 8.3 arises from the discontinuity between the Tremonti et al. (2004) mass–metallicity relationship and the Lee et al. (2006) low-mass extension (there is no gap in host galaxy masses as can be seen from Figure 4). Points are plotted by metallicity, and are corrected for redshift mass–metallicity effects as mentioned in the text, but the upper axis gives an approximate corresponding mass at zero redshift. Triangles are averages in 0.2 dex bins. Outer error bars are the standard deviation of the points in that bin, and the inner error bars are the errors on the mean.

(A color version of this figure is available in the online journal.)

cut are given in Table 2. The chosen cut parameters, and whether or not the cuts are made at all, do not affect the conclusions. We also study the effect of making a color correction, which corrects for dust, but also improperly corrects intrinsic luminosity dispersion. Such results give a lower limit on the dispersion of ^{56}Ni.

To make the color correction we followed the same steps as above, but first we use the color excess measured for each SN Ia to unredden the Hsiao et al. (2007) SED template using the Cardelli et al. (1989) law with $R_V = 1.8$ (Conley et al. 2007). We use a fiducial color of $c = 0$, where c is a linear combination of restframe $B-V$ and $U-B$ (Conley et al. 2008), roughly corresponding to $E(B-V)_0 = -0.057$ (Astier et al. 2006).

Mathematically, if $H_0(\lambda)$ is the unreddened template, then this process can be summed up by the following two equations:

$$f' = \frac{\int_{\lambda_1}^{\lambda_2} H(\lambda) d\lambda}{\int H_0(\lambda) d\lambda}, \quad (10)$$

and

$$F_{\rm bol} = \frac{\int_{\lambda_1}^{\lambda_2} S(\lambda) d\lambda}{f'}. \quad (11)$$

4. RESULTS

4.1. Galaxy Mass Versus SN Ia stretch

It is well known that SN lightcurve widths correlate with host galaxy morphology (Hamuy et al. 1995, 2000; Howell 2001; Gallagher et al. 2005), host color (Branch et al. 1996), or sSFR (Sullivan et al. 2006), in the sense that SNe with wider lightcurves are more commonly associated with late-type galaxies and vice versa. The fact that elliptical galaxies are generally larger (in a spatial sense) than spirals also may account for trends seen between lightcurve width and projected galactocentric distance (Wang et al. 1997; Gallagher et al. 2005). And while SN rates have been studied as a function of host galaxy mass (Mannucci et al. 2005; Sullivan et al. 2006), no study has examined lightcurve width as a function of host galaxy mass. Figure 4 shows such a comparison for SNLS SNe Ia. Keeping in mind that passive galaxies tend to have a high mass, the results are as expected from previous work—high-mass galaxies host few high-stretch SNe Ia, and low-mass galaxies host few low-stretch SNe Ia.

4.2. ^{56}Ni Mass Versus Host Galaxy Metallicity

In Figure 5, we have converted galaxy mass to gas-phase metallicity and converted integrated flux to ^{56}Ni mass as outlined in Section 3. We have overplotted the TBT03 relationship between metallicity and predicted SN Ia ^{56}Ni yield, corrected for O/Fe differences as outlined in Section 2. In this figure we make a color cut, but not a color correction. Figure 5 shows that there is a drop in average ^{56}Ni mass for SNe Ia from high-mass, high-metallicity (12+log(O/H) > 8.8) galaxies. TBT03 predicted a 25% difference in ^{56}Ni yield over a factor of 3 difference in progenitor metallicity. However, most of the effect occurred at metallicities 12+log(O/H) > 9.2 (see Figure 1), whereas most SNe Ia in this study occur in galaxies with lower metallicity. Figure 5 shows that the TBT03 prediction is fairly flat over the range of metallicities determined for actual SN hosts. Even when the steeper "thin disk" relation is used from Figure 1, at most, the expected effect is only 0.06 $M_\odot$ in this range. In comparison SNe Ia show a wide range in derived ^{56}Ni mass, here 0.2–1.0 $M_\odot$, though ranging from 0.1 to 1.3 $M_\odot$ for extreme cases such as SN 1991bg (Filippenko et al. 1992) and SNLS-03D3bb (Howell et al. 2006).

In other words, the TBT03 theory appears to be qualitatively consistent with observations, though there is additional scatter

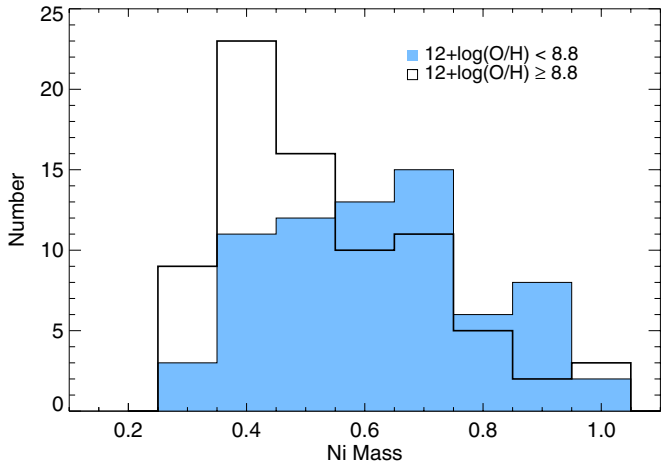

Figure 6. Histogram of SN ^{56}Ni mass split by inferred host gas-phase metallicity. Higher metallicity hosts have a lower ^{56}Ni yield, on average. This uses the non-color-corrected data from Figure 5.

(A color version of this figure is available in the online journal.)

not explained by the theory. An additional error of 0.16 $M_\odot$ of ^{56}Ni had to be added to the ^{56}Ni error bars in quadrature to achieve $\chi^2/\mathrm{DOF} = 1$.

Several SNe Ia with ^{56}Ni below 0.2 $M_\odot$ were conservatively eliminated with the color cut, on the grounds that extinction might be causing a low derived ^{56}Ni mass, although it is also possible that these are subluminous SNe, which have intrinsically redder colors (Garnavich et al. 2004).

Various effects can systematically alter the scaling of the observed ^{56}Ni mass in Figure 5, including changing the Hubble constant H_0 or the ratio of radiated to deposited radioactive decay energy γ, but these do not affect the overall results, because the normalization of the TBT03 prediction is arbitrary. Here, we have chosen the normalization by fitting to the data.

Another way to visualize the difference in ^{56}Ni yield between high- and low-metallicity galaxies is the histogram in Figure 6. Supernovae in more metal-rich hosts (12+log(O/H) > 8.8) have a much lower average ^{56}Ni yield than those in metal-poor hosts. The high-metallicity set has a peak in the distribution near 0.4 $M_\odot$, while the low-metallicity set peaks near 0.7 $M_\odot$. The probability that the ^{56}Ni yields from high- and low-metallicity hosts were drawn from the same distribution, according to the Kolmogorov–Smirnov (KS) test is 9×10^{-3}.

4.3. Reddening Correction

It is possible that the above results overestimate the scatter in SN Ia ^{56}Ni mass, if significant dust extinction remains after the color cut described in Section 3. To test this, we make the color correction in Figure 7. As expected, the scatter is reduced—now only 0.12 $M_\odot$ must be added in quadrature to the error bars to give $\chi^2/\mathrm{DOF} = 1$. Since this color correction includes an intrinsic SN Ia color correction as well as a dust correction, it will overcorrect the SN Ia magnitudes, but we do it to get an estimate of the limiting case. If SNe Ia are color corrected using $\beta = 2.8$ (Conley et al. 2007), the scatter is reduced to a range of 0.6 $M_\odot$ in ^{56}Ni for all but a few outliers. Thus the upper limit on the TBT03 metallicity effect is $0.06/0.6 = 10\%$.

4.4. Progenitor Age

Since there is an age–metallicity degeneracy, it is difficult to separate effects that may be caused by metallicity from

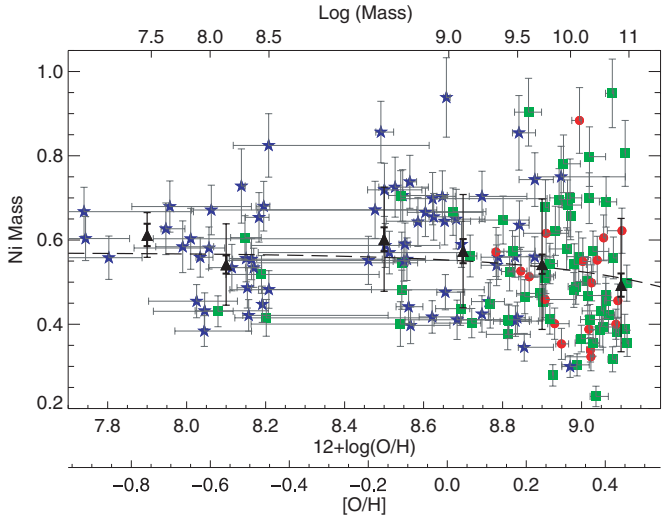

Figure 7. Same as Figure 5, but a color correction has been made. This correction would be appropriate if all SNe Ia were the same color, and all reddening and dimness were due to dust. However, there is an intrinsic color-luminosity relationship for SNe Ia that it is not currently possible to separate distinctly. Thus a color correction overcorrects the luminosity, and the result is a lower limit on the scatter in SN Ia ^{56}Ni mass.

(A color version of this figure is available in the online journal.)

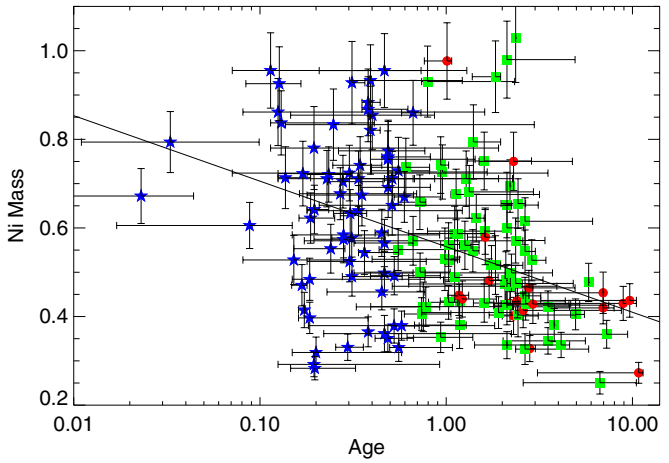

Figure 8. ^{56}Ni mass vs. host luminosity-weighted age as estimated from PEGASE.2 models. A color cut on the SN magnitudes has been made, but not a color correction. The line shows a fit to the data with slope -0.15 ± 0.03 and correlation coefficient -0.38.

(A color version of this figure is available in the online journal.)

those that may be caused by age of the progenitor. An age-brightness effect must exist for SNe Ia, since both SN rate and average luminosity are increased in young stellar populations (e.g., Howell 2001; Mannucci et al. 2005; Sullivan et al. 2006). Figure 8 confirms that there is a correlation between SN ^{56}Ni mass and host luminosity-weighted age as estimated from PEGASE.2 models—the slope of the line is significant at $\sim 5\sigma$. This correlation is understandably noisy—the PEGASE.2 luminosity-weighted age is merely an indicator of the mean age of an entire galaxy—the SN progenitor may have a very different age. Any age–brightness relation must be related to with the mass of the secondary star—in an old population more massive secondaries do not exist. But this is difficult to understand in the Chandrasekhar mass model—if all SNe Ia explode when the primary nears the Chandrasekhar mass, why should the mass

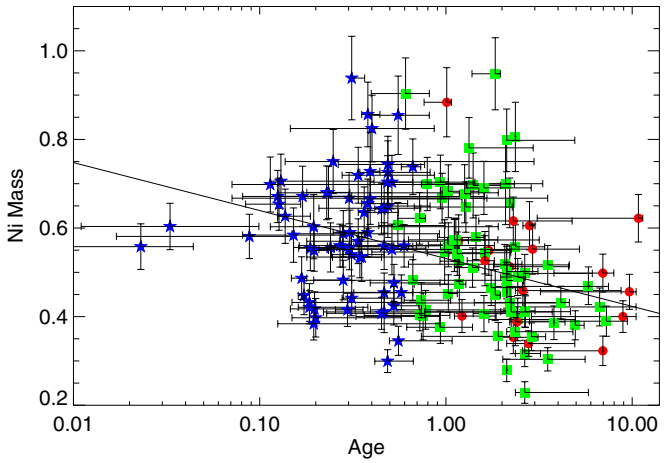

Figure 9. Same as Figure 8, but a color correction has been made. The line shows a fit to the data with slope -0.11 ± 0.028 and correlation coefficient -0.37.

(A color version of this figure is available in the online journal.)

of the secondary matter? This might be an indication that the binary evolution and mass transfer history, which is strongly dependent on the mass of the secondary, influences the outcome of the explosion.

Figure 9 shows the age-^{56}Ni mass relation after a color correction has been made. See Section 4.3 for a discussion of the trade-offs inherent in making this correction.

4.5. ^{56}Ni *Mass Versus Metallicity Grouped by Stretch*

Figure 10 shows ^{56}Ni mass versus 12+log(O/H) in three stretch bins. The most striking finding is that low-stretch ($s < 0.9$) SNe Ia almost exclusively occur in galaxies with high implied metallicity, roughly above solar. At the highest stretches ($s > 1.05$), the inferred ^{56}Ni mass is relatively insensitive to inferred host galaxy metallicity. Also, the scatter in ^{56}Ni mass is lower for low-stretch SNe Ia. This is likely due to several factors. For the low-stretch SNe, on the high side the ^{56}Ni mass is limited by the stretch cut, and on the low side it is limited by selection effects—it is difficult to find and spectroscopically confirm the lowest-stretch SNe. But there is also some evidence that SNe Ia in passive galaxies, which predominantly host low-stretch SNe Ia, make better standard candles (Sullivan et al. 2003). Some of this lower dispersion is likely due to lower dust extinction in these hosts, but it is also possible that moderately low-stretch SNe Ia are intrinsically more uniform as a population than high-stretch SNe Ia (Howell & Nugent 2004).

4.6. *Hubble Residuals*

G08 found a trend between SN Ia host galaxy metallicity and residuals from the Hubble diagram, indicating the lightcurve fitter used, MLCS2k2, cannot correct for the full range of SN Ia properties. Since the demographics of supernovae are known to evolve with redshift (Howell et al. 2007), any problem fully correcting SN Ia magnitudes could have dire consequences for SN Ia cosmology. Gallagher et al. cite a 9% systematic error in the measurement of the dark energy equation of state, w, larger than the current best statistical errors on w (Kowalski et al. 2008; Astier et al. 2006).

However, using our independent metallicity indicator and the SiFTO lightcurve fitter we find no systematic trend in Hubble residual versus inferred host galaxy metallicity. The results are shown in Figure 11, where the SNe Ia include those from

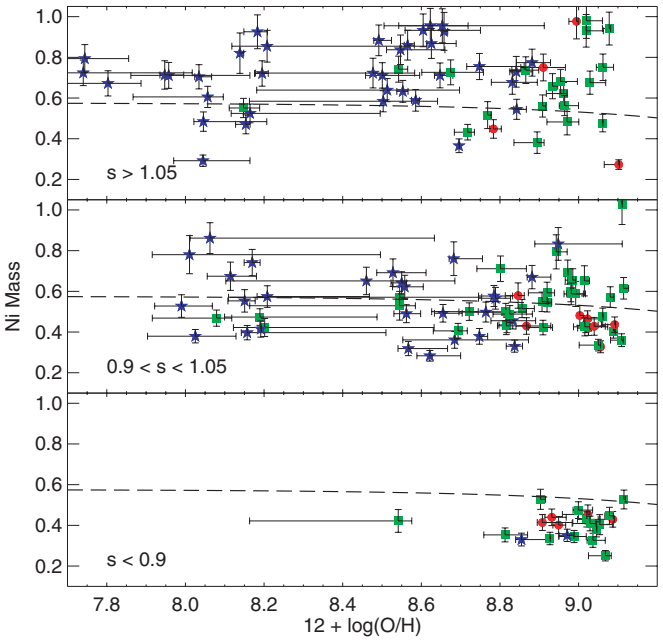

Figure 10. Ni mass vs. implied O/H as in Figure 5, split by stretch. Within a stretch bin there is no obvious inferred host galaxy metallicity dependency (line shows TBT03 prediction). The bottom panel shows that low-stretch SNe Ia are always produced in higher-metallicity galaxies, and the scatter in ^{56}Ni mass is lower for low-stretch SNe Ia.

(A color version of this figure is available in the online journal.)

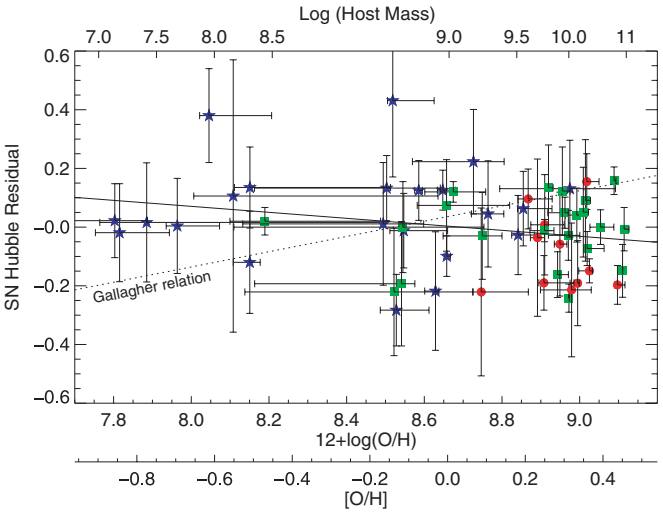

Figure 11. Hubble residual vs. inferred host galaxy metallicity for SNe Ia from the SNLS first-year sample (Astier et al. 2006). The solid line is a fit to the data, though it is consistent with zero slope at the $\sim 1\sigma$ level. The dotted line shows the G08 relation, here ruled out at $> 99.9\%$ confidence. The metallicity dispersion of 0.1 dex in the Tremonti et al. (2004) relation was added in quadrature when calculating the fit, but is not plotted for clarity. Residual errors do not include intrinsic SN Ia scatter about the Hubble line. No redshift or color cut was applied to the data; applying either or both gives a slope consistent with zero and still rules out the G08 relation at $> 99.9\%$ confidence. Symbol shapes and colors are the same as Figure 4. The upper axis shows the log mass for a galaxy with the metallicity found on the lower axis at $z = 0$. The convention used is the same as that in G08—overluminous SNe have a negative Hubble residual. Note that we are using an indicator of [O/H] as the independent variable, whereas Gallagher use an indicator of [Fe/H]. Any systematic trend with Hubble residual should show a slope with respect to either variable.

(A color version of this figure is available in the online journal.)

Astier et al. (2006) sample, but we apply no redshift or color cut. The solid line shows the best fit to the data, based on a Markov chain Monte Carlo analysis (LINMIX in IDL; Kelly 2007), which takes into account errors on the x-axis, and is

allowed to add extra scatter to the data (here 0.11 mag) to achieve the best fit. The slope of the best-fit line, -0.10 ± 0.07, is consistent with 0 at the $\sim 1\sigma$ level, and is inconsistent with the G08 slope of 0.26 at 5σ. In 10,000 Monte Carlo simulations, none produced a slope as steep at that found by G08.

Possible explanations for the difference between our results and those of G08 include that SiFTO can correct for differences in SN Ia properties that the current version of MLCS2k2 cannot, that one or the other metallicity indicator produces systematically flawed results, or that there are selection effects such that we are not comparing similar samples. We examine each hypothesis in turn.

SiFTO versus MLCS: Recently Jha et al. (2007) found evidence for a "Hubble Bubble"—local SNe Ia fit with MLCS2k2 give a different Hubble constant than do SNe Ia well into the Hubble flow. Wood-Vasey et al. (2007) considered this to be a 6% systematic error on w. However, Conley et al. (2007) did not see the same effect with either the SiFTO or SALT2 (Guy et al. 2007) lightcurve fitters, and traced the discrepancy to problems in the way MLCS2k2 handled dust extinction. MLCS2k2 assumed color excess beyond any assumed intrinsic SN Ia color relation is due to $R_V = 3.1$ (average Milky Way dust), though this appears not to be appropriate (SALT2 and SiFTO do an empirical fit to determine color–luminosity relationships). G08 do not provide enough information to determine whether a spurious reddening correction is driving their result.

Flawed metallicity indicators: Since we cannot make a definitive statement about whether the y-axis of Figure 11 (or the equivalent figure in G08) is flawed, the next culprit to examine is the x-axis. No metallicity indicator is perfect—the various caveats throughout the text attest to the limitations of our adopted method. Estimating a metallicity through a mass–metallicity relationship and determining the mass from photometry is certainly indirect. Still, it should be correct on average, especially since we are probing several orders of magnitude in mass, ranging from $< 10^8$ to $> 10^{11}$, and more than 1 dex in metallicity.

A stronger argument is that there seems to be no way to rearrange the points on the x-axis of Figure 11 to produce the G08 relation. On the other hand, it is possible to imagine that the x-axis of the upper left panel of G08 Figure 9 could be systematically flawed. The four points with the highest metallicity drive the relation. These four SNe all have E/S0 hosts with ages less than 3 Gyr, among the lowest in the G08 sample. Thus, the hosts of these SNe Ia are the most likely to have Hβ emission contaminating the Hβ absorption line index. Nominally this is used to determine age, but because of the age–metallicity degeneracy, it also affects the metallicity determination. As can be seen from G08 Figure 2, when the emission correction is applied 1/3 to 1/2 of their sample either falls off or is moved onto their theoretical age–metallicity grid. Even after correction, eight of their SNe Ia are more than 1σ too high off the grid, and their metallicities are extrapolations.

Selection effects: Since G08 target nearby SNe Ia in E/S0 hosts, they study many SNe Ia too dim to show up in a magnitude-limited sample like the SNLS. But the four SNe with high metallicities driving the G08 Hubble residual trend are all of normal magnitude $-19 < M_V < -19.5$, not the type absent from the SNLS sample. The metallicity range is also similar for the two studies, spanning a range $\pm \sim 0.5$ dex relative to solar. But if the differences between the two studies were due to some unknown selection effect, an important point is that it will not produce a systematic effect on cosmology, because the SNLS sample reflects cosmology as it is actually practiced, and we have shown that it produces unbiased Hubble residuals.

5. CONCLUSIONS

We find that host galaxies with a higher inferred metallicity produce SNe Ia with less ^{56}Ni on average. The effect proposed by TBT03, increased neutronization in higher metallicity environments, can qualitatively explain this trend, though there remains additional scatter in SN Ia luminosity that cannot be explained by the theory. TBT03 predict that SNe Ia in high-metallicity environments should be 25% dimmer than those in low-metallicity galaxies, though most of the dynamic range in this prediction occurs at metallicities several times solar. We have shown that SNLS supernovae occur in galaxies where the implied average metallicity is a few tenths of a dex above solar or below, and in this range the theory predicts only a 0.06 $M_\odot$ change in ^{56}Ni mass. The *average* ^{56}Ni yield does appear to decrease in metal-rich galaxies in accordance with the theory, but the large scatter (0.2–1.0 $M_\odot$, or ~ 0.6 $M_\odot$ with color correction), indicates that the theorized metallicity effect has at most a 7%–10% effect on ^{56}Ni yield.

The luminosity of SNe Ia appears to be dominated by other effects, possibly those caused by the age of the progenitor (Howell 2001; Gallagher et al. 2005; Mannucci et al. 2005; Sullivan et al. 2006). We find a correlation between host galaxy luminosity-weighted age and SN ^{56}Ni yield. This indicates that more massive stars (explicitly, massive secondaries, since they set the timescale for explosion in binaries), produce more luminous explosions, a result not well understood if most SNe Ia explode near the Chandrasekhar mass. We have also shown that allowing for changes in O/Fe with the metallicity [Fe/H] does not have a major effect on the theoretical prediction of TBT03 for metallicities within the observed range of our sample, so long as one is using the O/H as the independent variable.

Unlike G08, we find no trends between residuals from the Hubble diagram and host metallicity. We conclude that metallicity is not a significant systematic error for the measurement of w. The G08 finding may be due to problems with their lightcurve fitter, MLCS2k2, or with their method of host metallicity determination which relies on an uncertain correction for Hβ emission, and the extrapolation of theoretical models to cover the host galaxies of SNe Ia which fall off the grid.

These findings are broadly consistent with the range of local SN Ia host galaxy metallicities found by Gallagher et al. (2005), though we differ in how we compare the model to the data, and in the interpretation of the results. Despite using completely different methodology and data, both studies find that the majority of SN hosts have a metallicity between $8.4 < \log(\mathrm{O/H}) + 12 < 9.1$. Additionally we find several lower metallicity, low-mass hosts. These are underrepresented in low redshift searches which target large, higher-mass galaxies (e.g., Li et al. 2001). But rather than convert the observations to ^{56}Ni mass, Gallagher et al. (2005) converted the TBT03 model prediction into an expected difference in Δm_{15} (Phillips 1993). They found a fairly steep evolution in the Δm_{15} model prediction over the observed range in host O/H, in contrast to the flat prediction over the same range found here (Figure 5) and in TBT03. This is because they used the delayed detonation models of Höflich et al. (2002) and the empirical relations of Garnavich et al. (2004) to convert the model to the observed parameter Δm_{15}. The Höflich et al. (2002) models had a varying detonation transition density, so Gallagher

et al. (2005) found a steeper relation than one would derive if only O/H were varied while holding the other properties of the explosion fixed. As a result, they concluded that the TBT03 prediction is a poor fit to the data, whereas we find that it could account for some of the variation in SN Ia properties, but it is not the dominant effect.

Our findings are also consistent with Piro & Bildsten (2008), who roughly estimated that the TBT03 theory could only explain a small fraction of SN Ia luminosity based on average SNLS SN Ia stretches reported in Howell et al. (2007) and average SN host metallicity estimated from the galaxy types in Sullivan et al. (2006).

One caveat regarding our findings is that we are using a proxy for the global average galaxy metallicity—we have no way of knowing the actual progenitor's metallicity. One could imagine an effect that would skew the results, such as an enhanced SN rate in metal-poor or metal-rich environments, or similar diminution of the rate in either environment, such that the average SN metallicity would not be representative of the average metallicity in the galaxy. While there has been speculation from time to time that such effects could in principle exist (Kobayashi et al. 1998; Langer et al. 2000), there is no observational evidence that they do.

The absolute calibration of the mass–metallicity relationship is also uncertain (Kewley & Ellison 2008), but changing it would have the main effect of moving all points in Figure 5 to slightly lower or higher metallicities. Our conclusions would remain unchanged—that the metallicity effect can only account for a fraction of the scatter in SN Ia luminosities.

Piro & Bildsten (2008) find that weak reactions during low-level burning in the white dwarf in the ~ 1000 years leading up to explosion (i.e., simmering) may increase the neutron excess. This effect may set a "floor" to the level of neutronization that dominates over the TBT03 metallicity effect at low metallicities $Z/Z_{\odot} \lesssim 2/3$. Chamulak et al. (2008) also find that simmering can increase neutronization. Since neutronization effects during simmering depend on the degree of simmering, and at least to first order do not appear to depend on metallicity, it is possible that simmering could wash out the TBT03 metallicity effect. Significant uncertainties, including the role of the convective Urca process, remain, and further study is required. At the very least it seems that simmering cannot enhance the TBT03 metallicity effect enough to account for the significant scatter in SN Ia luminosities (Piro & Bildsten 2008).

One additional caveat is that it is possible that a change in metallicity could alter the explosion mechanism itself, not just whether the process produces more ^{56}Ni or ^{58}Ni. Chamulak et al. (2007) found that laminar flame speed also depends on the metallicity, but this is probably a higher-order effect. At any rate, this process is so poorly understood that it is not yet possible to test this effect with observations.

The authors thank Lars Bildsten, Kevin Bundy, and Renbin Yan for helpful discussions. We also thank the Kavli Institute for Theoretical Physics, and the Aspen Center for Physics, where the initial development of this work was done. This research was supported in part by the National Science Foundation under grant no PHY05-51164.

E.F.B is supported by grant AST-0507456 from the National Science Foundation. M.S. acknowledges support from the Royal Society. J.C.W. is supported in part by NSF AST-0707769.

The SNLS collaboration gratefully acknowledges the assistance of Pierre Martin and the CFHT Queued Service Observations team. Canadian collaboration members acknowledge support from NSERC and CIAR; French collaboration members from CNRS/IN2P3, CNRS/INSU, and CEA.

The SNLS relies on observations with MegaCam, a joint project of CFHT and CEA/DAPNIA, at the Canada–France–Hawaii Telescope (CFHT) which is operated by the National Research Council (NRC) of Canada, the Institut National des Science de l'Univers of the Centre National de la Recherche Scientifique (CNRS) of France, and the University of Hawaii. This work is based in part on data products produced at the Canadian Astronomy Data Centre as part of the Canada–France–Hawaii Telescope Legacy Survey, a collaborative project of the National Research Council of Canada and the French Centre National de la Recherche Scientifique.

REFERENCES

Arnett, W. D. 1979, ApJ, 230, L37
Arnett, W. D. 1982, ApJ, 253, 785
Asplund, M., Grevesse, N., & Sauval, A. J. 2005, in ASP Conf. Ser. 336, Cosmic Abundances as Records of Stellar Evolution and Nucleosynthesis, ed. T. G. Barnes, III & F. N. Bash (San Francisco, CA: ASP), 25
Astier, P., et al. 2006, A&A, 447, 31
Badenes, C., Bravo, E., & Hughes, J. P. 2008, ApJ, 680, L33
Baumont, S., et al. 2008, A&A, in press (astro-ph/0809.4407)
Bensby, T., & Feltzing, S. 2006, MNRAS, 367, 1181
Blinnikov, S. I., Röpke, F. K., Sorokina, E. I., Gieseler, M., Reinecke, M., Travaglio, C., Hillebrandt, W., & Stritzinger, M. 2006, A&A, 453, 229
Branch, D. 1992, ApJ, 392, 35
Branch, D., & Khokhlov, A. M. 1995, Phys. Rep., 256, 53
Branch, D., Romanishin, W., & Baron, E. 1996, ApJ, 465, 73
Bronder, T. J., et al. 2008, A&A, 477, 717
Cardelli, J. A., Clayton, G. C., & Mathis, J. S. 1989, ApJ, 345, 245
Chamulak, D. A., Brown, E. F., & Timmes, F. X. 2007, ApJ, 655, L93
Chamulak, D. A., Brown, E. F., Timmes, F. X., & Dupczak, K. 2008, ApJ, 677, 160
Chiappini, C., Romano, D., & Matteucci, F. 2003, MNRAS, 339, 63
Cid Fernandes, R., Mateus, A., Sodré, L., Stasińska, G., & Gomes, J. M. 2005, MNRAS, 358, 363
Colgate, S. A., & McKee, C. 1969, ApJ, 157, 623
Colgate, S. A., Petschek, A. G., & Kriese, J. T. 1980, ApJ, 237, L81
Commins, E. D. 2004, New Astron. Rev., 48, 567
Conley, A., Carlberg, R. G., Guy, J., Howell, D. A., Jha, S., Riess, A. G., & Sullivan, M. 2007, ApJ, 664, L13
Conley, A., et al. 2006, AJ, 132, 1707
Conley, A., et al. 2008, ApJ, 681, 482
Contardo, G., Leibundgut, B., & Vacca, W. D. 2000, A&A, 359, 876
Elias-Rosa, N., et al. 2008, MNRAS, 384, 107
Ellis, R. S., et al. 2008, ApJ, 674, 51
Filippenko, A. V., et al. 1992, AJ, 104, 1543
Fioc, M., & Rocca-Volmerange, B. 1997, A&A, 326, 950
Fioc, M., & Rocca-Volmerange, B. 1999, arXiv:astro-ph/9912179
Foley, R. J., Filippenko, A. V., & Jha, S. W. 2008, ApJ, 686, 117
Gallagher, J. S., Garnavich, P. M., Berlind, P., Challis, P., Jha, S., & Kirshner, R. P. 2005, ApJ, 634, 210
Gallagher, J. S., Garnavich, P. M., Caldwell, N., Kirshner, R. P., Jha, S. W., Li, W., Ganeshalingam, M., & Filippenko, A. V. 2008, ApJ, 685, 752
Garnavich, P. M., et al. 2004, ApJ, 613, 1120
Guy, J., et al. 2007, A&A, 466, 11
Hamuy, M., Phillips, M. M., Maza, J., Suntzeff, N. B., Schommer, R. A., & Aviles, R. 1995, AJ, 109, 1
Hamuy, M., Trager, S. C., Pinto, P. A., Phillips, M. M., Schommer, R. A., Ivanov, V., & Suntzeff, N. B. 2000, AJ, 120, 1479
Hatano, K., Branch, D., & Deaton, J. 1998, ApJ, 502, 177
Höflich, P., Gerardy, C. L., Fesen, R. A., & Sakai, S. 2002, ApJ, 568, 791
Höflich, P., & Khokhlov, A. 1996, ApJ, 457, 500
Höflich, P., Wheeler, J. C., & Thielemann, F. K. 1998, ApJ, 495, 617
Howell, D. A. 2001, ApJ, 554, L193
Howell, D. A., Höflich, P., Wang, L., & Wheeler, J. C. 2001, ApJ, 556, 302
Howell, D. A., & Nugent, P. 2004, in Cosmic Explosions in Three Dimensions: Asymmetries in Supernovae and Gamma-ray Bursts (Cambridge: Cambridge Univ. Press), 151
Howell, D. A., Sullivan, M., Conley, A., & Carlberg, R. 2007, ApJ, 667, L37

Howell, D. A., et al. 2005, ApJ, 634, 1190
Howell, D. A., et al. 2006, Nature, 443, 308
Howell, D. A., Wang, L., & Wheeler, J. C. 2000, ApJ, 530, 166
Hsiao, E. Y., Conley, A., Howell, D. A., Sullivan, M., Pritchet, C. J., Carlberg, R. G., Nugent, P. E., & Phillips, M. M. 2007, ApJ, 663, 1187
Ivanov, V. D., Hamuy, M., & Pinto, P. A. 2000, ApJ, 542, 588
Jha, S., Riess, A. G., & Kirshner, R. P. 2007, ApJ, 659, 122
Junde, H. 1999, Nucl. Data Sheets, 86, 315
Kasen, D., Nugent, P., Thomas, R. C., & Wang, L. 2004, ApJ, 610, 876
Kasen, D., & Woosley, S. E. 2007, ApJ, 656, 661
Kelly, B. C. 2007, ApJ, 665, 1489
Kewley, L. J., & Dopita, M. A. 2002, ApJS, 142, 35
Kewley, L. J., & Ellison, S. L. 2008, ApJ, 681, 1183
Khokhlov, A., Mueller, E., & Hoeflich, P. 1993, A&A, 270, 223
Kobayashi, C., Tsujimoto, T., Nomoto, K., Hachisu, I., & Kato, M. 1998, ApJ, 503, L155
Kowalski, M., et al. 2008, ApJ, 686, 749
Krisciunas, K., et al. 2007, AJ, 133, 58
Langer, N., Deutschmann, A., Wellstein, S., & Höflich, P. 2000, A&A, 362, 1046
Le Borgne, D., & Rocca-Volmerange, B. 2002, A&A, 386, 446
Lee, H., Skillman, E. D., Cannon, J. M., Jackson, D. C., Gehrz, R. D., Polomski, E. F., & Woodward, C. E. 2006, ApJ, 647, 970
Lentz, E. J., Baron, E., Branch, D., & Hauschildt, P. H. 2001, ApJ, 557, 266
Leonard, D. C., Li, W., Filippenko, A. V., Foley, R. J., & Chornock, R. 2005, ApJ, 632, 450
Li, W., Filippenko, A. V., Treffers, R. R., Riess, A. G., Hu, J., & Qiu, Y. 2001, ApJ, 546, 734
Liang, Y. C., Yin, S. Y., Hammer, F., Deng, L. C., Flores, H., & Zhang, B. 2006, ApJ, 652, 257
Mannucci, F., della Valle, M., Panagia, N., Cappellaro, E., Cresci, G., Maiolino, R., Petrosian, A., & Turatto, M. 2005, A&A, 433, 807
Mazzali, P. A., Nomoto, K., Cappellaro, E., Nakamura, T., Umeda, H., & Iwamoto, K. 2001, ApJ, 547, 988
Nugent, P., Baron, E., Branch, D., Fisher, A., & Hauschildt, P. H. 1997, ApJ, 485, 812
Nugent, P., Branch, D., Baron, E., Fisher, A., Vaughan, T., & Hauschildt, P. H. 1995, Phys. Rev. Lett., 75, 394
Perlmutter, S., et al. 1997, ApJ, 483, 565
Perlmutter, S., et al. 1999, ApJ, 517, 565
Phillips, M. M. 1993, ApJ, 413, L105
Phillips, M. M., Lira, P., Suntzeff, N. B., Schommer, R. A., Hamuy, M., & Maza, J. 1999, AJ, 118, 1766
Pinto, P. A., & Eastman, R. G. 2000a, ApJ, 530, 744
Pinto, P. A., & Eastman, R. G. 2000b, ApJ, 530, 757
Piro, A. L., & Bildsten, L. 2008, ApJ, 673, 1009
Prieto, J. L., Stanek, K. Z., & Beacom, J. F. 2008, ApJ, 673, 999
Ramírez, I., Allende Prieto, C., & Lambert, D. L. 2007, A&A, 465, 271
Riess, A. G., et al. 1998, AJ, 116, 1009
Riess, A. G., et al. 1999, AJ, 118, 2675
Riess, A. G., Press, W. H., & Kirshner, R. P. 1996, ApJ, 473, 88
Sauer, D. N., et al. 2008, MNRAS, 391, 1605
Savaglio, S., et al. 2005, ApJ, 635, 260
Stritzinger, M., Mazzali, P. A., Sollerman, J., & Benetti, S. 2006, A&A, 460, 793
Sullivan, M., et al. 2003, MNRAS, 340, 1057
Sullivan, M., et al. 2006, ApJ, 648, 868
Timmes, F. X., Brown, E. F., & Truran, J. W. 2003, ApJ, 590, L83
Trager, S. C., Faber, S. M., Worthey, G., & González, J. J. 2000, AJ, 119, 1645
Tremonti, C. A., et al. 2004, ApJ, 613, 898
Truran, J. W., Arnett, W. D., & Cameron, A. G. W. 1967, Can. J. Phys., 45, 2315
van den Bergh, S. 1997, AJ, 113, 197
Vila Costas, M. B., & Edmunds, M. G. 1993, MNRAS, 265, 199
Wang, L., Höflich, P., & Wheeler, J. C. 1997, ApJ, 483, L29
Wang, L., Wheeler, J. C., Li, Z., & Clocchiatti, A. 1996, ApJ, 467, 435
Wang, X., et al. 2008, ApJ, 675, 626
Wheeler, J. C., Sneden, C., & Truran, Jr. 1989, ARA&A, 27, 279
Wood-Vasey, W. M., et al. 2007, ApJ, 666, 694